Global NEST Journal, Vol 23, No 2, pp 323-332

Enhanced photocatalytic degradation of Remazol Black under visible light illumination through S doped TiO_2 (S-TiO_2) nanoparticles: operational factors and kinetic study

Dwiyanna R., Roto R., Suwondo K.P. and Wahyuni E.T.*

Department of Chemistry, Faculty of Mathematics and Natural Sciences, Universitas Gadjah Mada – Sekip Utara, Bulaksumur, Yogyakarta, 55281, Indonesia

Received: 06/03/2021, Accepted: 23/07/2021, Available online: 15/08/2021

*to whom all correspondence should be addressed: e-mail: endang_triw@ugm.ac.id

https://doi.org/10.30955/gnj.003586

Graphical abstract

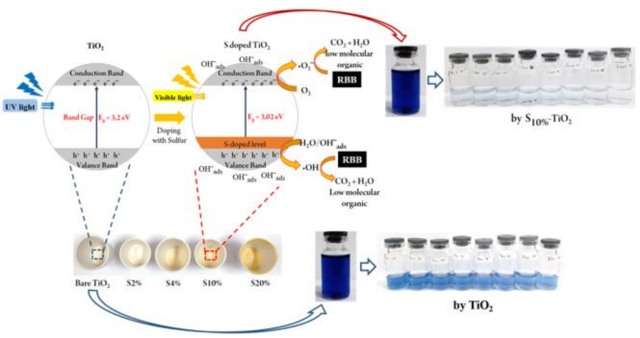

Abstract

The degradation of Remazol Black (RBB) by S-TiO_2 photocatalyst was investigated. X-ray diffraction, fourier-transform infrared spectroscopy, scanning electron microscopy, transmission electron microscopy, and UV-vis specular reflectance spectroscopy has been used to characterize S-TiO_2. The results suggested that the optical absorption edge of TiO_2 was red-shifted by the addition of S dopants and the bandgap energy was 3.02 eV. The sulfur species were found to be evenly dispersed on the TiO_2 crystal lattice as cationic sulfur (S^{6+}) which corresponds to the cationic substitution on TiO_2. The particle size decreased to 4-14 nm after S doping, which indicates that the addition of S dopants has contributed to an improvement in the photocatalyst surface area. The degradation of RBB was achieved 94% after 120 min visible light irradiation, a remarkable increase compared to bare TiO_2 which was only able to degrade 48% of RBB at the same time. Optimization of the pH showed that the optimum pH for RBB degradation was 3.0, and the photocatalyst dose was 0.8 g L^{-1}. Kinetic study showed that S-TiO_2 photocatalytic degradation of RBB followed the pseudo-second-order kinetics model. Reducing the bandgap has been found to increase the activity of photodegradation in the visible light region.

Keywords: Kinetic, photocatalyst, photodegradation, remazol black, S-TiO_2.

1. Introduction

Water pollution, along with the increasing production of industrial wastewater, has become a concern all over the world, which reduces the availability of clean water for living beings. Dyes wastewater from textile, paper, and leather industries are the main problem of contamination in the aquatic environment. Reactive dyes are the most commonly used (60-70%) among various type of synthetic dyes due to low energy consumption in the dyeing process, water fastness, and color brightness (Marques *et al.*, 2010; Ahmad and Rahman, 2011). Reactive dyes, such as Remazol Black, consist of one or more azo bonds (−N=N−) attached to aromatic ring (Rauf *et al.*, 2011; Ghoreishian *et al.*, 2014). The complex chemical structure makes this dye stable and difficult to biodegrade and the concentration in the environment tends to persist if this dye enters the water bodies (Chen *et al.*, 2012; Akti, 2018). Meanwhile, the negative effects of this dye on humans and aquatic animals have been reported due to its toxic and carcinogenic properties (Aksu and Akın, 2010; Sahel *et al.*, 2010, 2014). Thus, an effective method is needed to remove the concentration of this dye from wastewater before being discharged into the environment.

It has been found that advanced oxidation processes (AOPs) are one of the most promising and efficient technologies for treating dyes in wastewater. This method has gained considerable attention because it is simple to handle and significantly produces lower residues compared to the conventional treatment process (Rauf *et al.*, 2011; Alvarez *et al.*, 2018; Pereira *et al.*, 2019) Among other AOPs methods, TiO_2 heterogenous photocatalyst is the most extensively studied and used due to its advantages such as high photocatalytic activity for the decomposition of organic pollutants, chemical stability, non-toxicity, and low cost (Muruganandham and Swaminathan, 2006; Yilmaz *et al.*, 2017; Islam *et al.*, 2020; Wahyuni *et al.*, 2020). TiO_2 can generate highly reactive hydroxyl radicals (•OH) which have very high oxidizing power compared to other oxidants to degrade recalcitrant organic contaminants in wastewater (Bessergenev *et al.*, 2015; Eskandari *et al.*, 2019). Nontheless, TiO_2 has restrictions in its application. In order to generate hydroxyl radicals, TiO_2 must be exposed to photons from electromagnetic radiation with an energy greater than the bandgap energy of TiO_2 (3.2 eV for anatase). Such photons are available in the ultraviolet (UV) region, whereas only about 5% of the sunlight UV rays can be utilized for the photocatalytic process (Han *et al.*, 2011; Z. Chen *et al.*, 2017; Wu *et al.*, 2018), as well as the high recombination rate of the electron-hole during illumination (Murcia *et al.*, 2015; Siddiqa *et al.*, 2015; Isari *et al.*, 2018), which reduces the photocatalytic activity of TiO_2. To overcome these limitations, TiO_2 modification is required to enhance photocatalytic activity under visible light illumination.

The addition of metal or non-metal ions dopant into TiO_2 lattice is an effective attempt to shift the TiO_2 adsorption edge from UV to visible region (Asiri *et al*., 2014; Chaudhuri and Paria, 2014; Mcmanamon *et al*., 2015). Doping with non-metal ions has been considered to be one of the most promising methods to extend the visible light response of TiO_2 (Tian *et al*., 2009; Marques *et al*., 2010). Compared to other non-metals, sulfur is a good candidate due to bandgap manipulation, high thermal stability, and adequate the photocatalytic activity in visible light illumination (Zhu *et al.*, 2015; Lin *et al.*, 2016; X. Chen *et al.*, 2017). All oxidation states of sulfur dopants both cationic (S^{6+}) and anionic (S^{2-}) may exist in the TiO_2 lattice depending on the synthesis condition or the precursors of sulfur, and substitute Ti or O ions in the TiO_2 structure, resulting in impurity state near to the conduction band (CB), bandgap narrowing, and increasing TiO_2 response to visible light (Szatmáry *et al*., 2011; Devi and Kavitha, 2014; Abu and Ribeiro, 2016; Olowoyo *et al*., 2018). S dopant can also be an electron trap that slows down the recombination rate, extending the lifetime of the hydroxyl radicals, and showing high photocatalytic activity (Abu and Ribeiro, 2016). Various methods have been studied for doping S into TiO_2, such as solvothermal (Kumar *et al*., 2016), sol-gel (Devi and Kavitha, 2014; Han *et al*., 2014), oxidant peroxide (Abu and Ribeiro, 2016), sonothermal (Olowoyo *et al*., 2018), hydrothermal (Kumar et al., 2016), co-hydrolysis precipitation (Chen *et al*., 2019). Among these methods, sol-gel is one of the most widely used because the ability to controlling particle size, morphology, homogeneity, resulting in high crystallinity and surface area (Hamadanian and Majedi, 2009; Siddiqa *et al*., 2015).

To the best of our knowledge, no studies have been reported on the photocatalytic decontamination study of Remazol Black over S-TiO_2 photocatalyst prepared via sol-gel method under visible light illumination. Furthermore, we developed the utilization of light-emitting diodes (LED) as the light source due to their long lifetime and high energy efficiency compared to the common types of the light sources such as Xe lamps and Hg-Xe lamps (Eskandari *et al*., 2019). To assess the optimum condition, the effects of the operational parameters on the decolorization efficiency were evaluated. Subsequently, the kinetics of the photodegradation of Remazol Black using S-doped TiO_2 photocatalyst were also studied.

2. Materials and methods

2.1. Materials

All chemicals used in this study were analytical grade and were used without any further purification. Titanium(IV) isopropoxide (TTIP, 97%) was obtained from Hangzhou Jiu Peng Material Co., Ltd. (China). Thiourea (CH_4N_2S), ethanol absolute (C_2H_5OH), hydrochloric acid (HCl, 36%), sodium hydroxide (NaOH), and Remazol Black (RBB, $C_{26}H_{21}O_{19}N_5S_6Na_4$, MW= 991.82 g mol^{-1}) were purchased from Merck, and deionized water was used in this work. The chemical structure of RBB is shown in Figure 1.

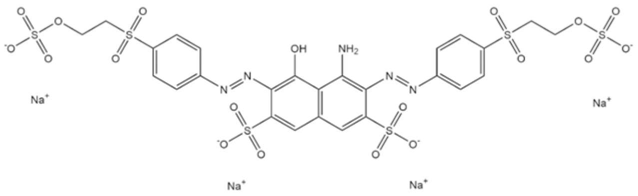

Figure 1. Chemical structure of Remazol Black (RBB)

2.2. Synthesis of S-TiO_2 photocatalyst

S-TiO_2 photocatalyst was synthesized by the sol-gel method. Initially, a stoichiometric amount of titanium(IV) isopropoxide was dissolved in ethanol absolute under magnetic stirring. At the same time, 0.114 g of thiourea was dissolved in a mixture of distilled water and ethanol (volume ratio 1:1) to get the desired ratio of 2% (w/w) Ti:S dopant concentration. This solution was added dropwise to the TTIP solution under magnetic stirring, and the pH of the solution was adjusted to 3.0 by the addition of 1 M HCl. Stirring was continued for 2 h, then the final mixed solution was aged for 24 h. Next, the gels were dried at 80 ^oC for 4 h to evaporate water and organic materials. Finally, dry gels were calcined in a muffle furnace at 450 ^oC for 3 h to control the crystal phase of the catalyst. The resulting catalyst was ground thoroughly and labeled as $S_{2\%}$-TiO_2. A similar procedure was followed to prepare S-TiO_2 with a concentration ratio of 4%, 10%, 20%, and bare TiO_2 without the addition of sulfur dopants.

2.3. Characterization

X-ray diffractometer (XRD Shimadzu 6000, Cu Kα radiation λ = 0.15406 nm as the source of X-rays, operated at 40 kV, 30 mA, the angular range of 2θ = 5-90^o and nickel as the filter) was used to identify composition and crystalline phase of the photocatalyst. The crystallite size was calculated by Scherrer equation (eq. 1):

$$D = \frac{k}{\beta \cos\theta} \quad (1)$$

where k is a shape factor (0.94), λ is the wavelength of Cu Kα source used, β is the full width at half maximum (FWHM), and θ is the angle of diffraction.

To verify the functional groups and chemical bonds contained in the photocatalyst, Fourier-Transform

Infrared (FTIR) spectrophotometer (Shidmazu Prestige 21) was used in the wavenumber 4000-400 cm^{-1}. The morphology of the nanoparticles was measured by Scanning Electron Microscopy (SEM) and Transmission Electron Microscopy (TEM, Jeol Jem-1400), which the composition of the nanoparticles was analyzed by Energy Dispersive X-ray (EDX). UV-vis Specular Reflectance Spectroscopy (UV-vis SRS) was used to identify photocatalyst light absorption profiles.

2.4. Photocatalytic activity

The photodegradation of RBB was carried out in a self-constructed photoreactor (Figure 2), with a batch system in a close reactor equipped with 4 UV lamps (@20W, 200 lm/m^2) and 4 visible lamps (TL-D, @20W, 2000 lm/m^2) as light sources. The variable parameters were investigated, including different types of photocatalyst, initial pH, catalyst dosage, dye concentration, and the light source. The pH of the solution was adjusted by the addition of HCl or NaOH, and the pH was determined using a pH meter (Schott Lab 860 Laboratory). In each test, several photocatalysts were dispersed in the RBB solution. Before irradiation, the suspension was magnetically stirred in the dark for 30 min to achieve the adsorption-desorption equilibrium. Then, the photocatalytic reaction was initiated by exposing the suspension to the light source under continous stirring. Samples with certain time intervals were taken from the reactor and centrifuged at 5000 rpm for 10 min to separate the photocatalyst from the solution. The residual RBB concentration was determined using the UV-Vis spectrophotometer (Analytic JENA Double Beam/Specord 200 Plus) at 598 nm. The removal efficiency was calculated using Eq. (2):

$$\text{The removal efficiency of RBB (\%)} = \frac{C_i - C_f}{C_f} \times 100 \qquad (2)$$

where C_i was the initial concentration (mg L^{-1}) and C_f was the final concentration (mg L^{-1}).

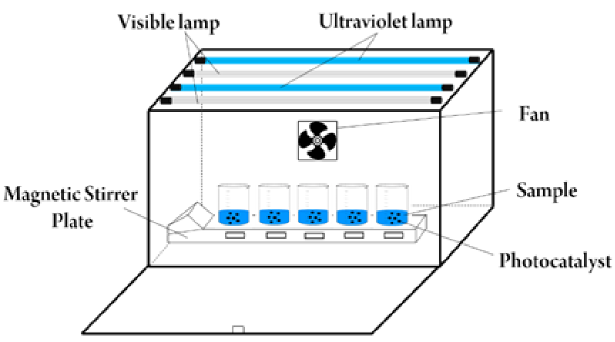

Figure 2. Schematic diagram of the reactor for photocatalytic activity measurement

3. Result and Discussion

3.1. Photocatalyst characterization

3.1.1. XRD analysis

The crystal phase of the synthesized-photocatalyst was analyzed by XRD and the diffraction patterns of TiO_2 and S-TiO_2 photocatalysts calcined at 450 °C showed in Figure 3. All photocatalysts exhibit peaks at 2θ 25.21, 37.73, 47.95, 53.87, 54.97, 62.66, and 75.12, which correspond to the diffraction of the (101), (004), (200), (105), (211), (204), and (215) anatase TiO_2 (JCPDS No. 21-1272) (Z. Chen *et al.*, 2017). The absence of rutile phase indicated that the anatase TiO_2 was successfully synthesized. As shown in Figure 3 (b)-(e), S dopant does not change the crystal phase of TiO_2. The average crystallite size was estimated using Scherrer's equation (Eq. 1) and the results were shown in Table 1.

Table 1. The average crystallite sizes of TiO_2 and S-TiO_2

Photocatalyst	*D* (nm)
TiO_2	5.15
$S_{2\%}$-TiO_2	2.82
$S_{4\%}$-TiO_2	3.05
$S_{10\%}$-TiO_2	3.50
$S_{20\%}$-TiO_2	9.17

Generally, samples with S dopant concentration lower than 20% showed the decrease in the average crystallite sizes. It might be due to the S atoms incorporating into the TiO_2 lattices, which could inhibit the crystal growth. In contrast, the increase of the S dopant concentration up to 20% causing the agglomeration on the TiO_2 surfaces or crystals and thus, enchancing the crystallite size of $S_{20\%}$-TiO_2 sample.

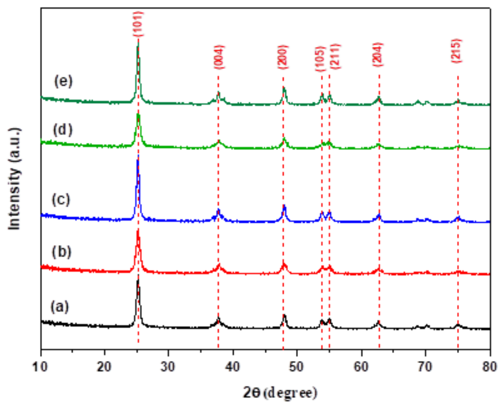

Figure 3. XRD patterns of photocatalyst (a) TiO_2, (b) $S_{2\%}$-TiO_2, (c) $S_{4\%}$-TiO_2, (d) $S_{10\%}$-TiO_2, and (e) $S_{20\%}$-TiO_2 respectively

3.1.2. FT-IR analysis

FT-IR spectrum was applied to determine the functional groups presented in the photocatalyst. Figure 4 shows that on bare TiO_2 sample, the broad absorption bands at 3400-3600 and 1635 cm^{-1} attribute to the stretching and bending vibration of the hydroxyl group on the TiO_2 surface (Yi *et al.*, 2019). Then, the adsorption peaks at 2924 cm^{-1} indicate the vibration of the TiO_2-OH group and the peaks at 500-800 cm^{-1} assign to the bending vibration of Ti−O which corresponds to the literature (Chen *et al.*, 2019).

After the S-doping, the absorption intensity at 3400-3600 cm^{-1} and 1635 cm^{-1} was much stronger than bare TiO_2, because the replacement of Ti^{4+} by S^{6+} ions caused imbalance due to an excess of positive charges on the surface of the catalyst. Numerous hydroxide ions are attracted to the surface of the catalyst due to the charge imbalance. This result in hydroxyl radicals are more adsorbed on the highly reactive surface of the adsorbent (Devi and Kavitha, 2014). Meanwhile, the absorption bands for Ti−O bending vibration became broader, which implies that the Ti−O−Ti bond has weakened due to the replacement of Ti^{4+} by cationic S, confirmed by the presence of a new characteristic peak at 1049-1080 cm^{-1} that corresponded to Ti−O−S bending vibration (Chen *et al.*, 2017; Chen *et al.*, 2019). Besides, the peak at 1110-1126 cm^{-1} confirmed the S−O bending vibration in the form of SO_4^{2-}, indicated that sulfur present in cationic species (S^{6+}). This is also evidenced by the absence of a peak at 1135 cm^{-1} for the Ti−S bond formed from the substitution of O^{2-} by anionic sulfur (S^{2-}). Compared to the substitution of O^{2-} by S^{2-}, the substitution of Ti^{4+} by S^{6+} is chemically more favorable since the ionic radius of S^{2-} (1.7 Å) is quite larger than O^{2-} (1.22 Å), which cause the bond formation of the Ti−S by O^{2-} substitution will require more energy and is difficult to achieve compared to the substitution of Ti^{4+} by S^{6+}. The FTIR spectrum shows that the incorporation of S dopant into TiO_2 has been successfully carried out.

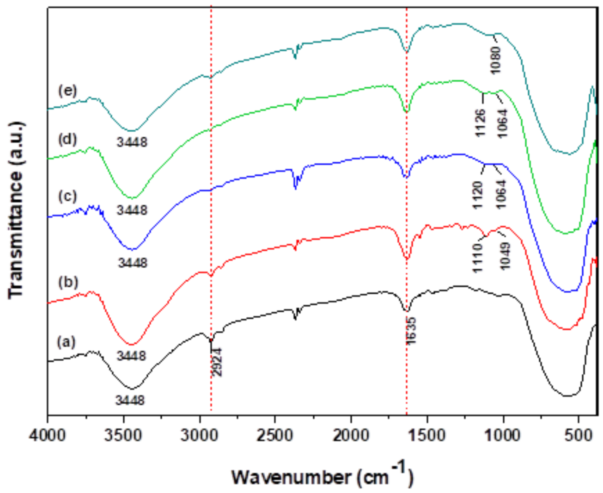

Figure 4. FT-IR spectra of (a) TiO_2, (b) $S_{2\%}$-TiO_2, (c) $S_{4\%}$-TiO_2, (d) $S_{10\%}$-TiO_2, and (d) $S_{20\%}$-TiO_2

3.1.3. SEM analysis

The surface morphology of photocatalyst was analyzed using SEM. As can be seen in Figure 5, both TiO_2 and S-TiO_2 nanoparticles show a spherical morphology and uniform particle size homogeneity. In addition, the morphology of TiO_2 nanoparticles did not change by the incorporation of S into TiO_2. Then, EDX analysis was employed to verify the presence of S element in the samples and the results showed that the major peaks in bare TiO_2 were Ti and O elements. The S element was observed in $S_{10\%}$-TiO_2 and $S_{20\%}$-TiO_2 samples, indicating S-doped TiO_2 formation. However, The S element could not be identified in $S_{2\%}$-TiO_2 and $S_{4\%}$-TiO_2 samples, which may be caused by the low S concentration addition. The EDX spectrum of TiO_2 and S-TiO_2 are shown in Figure 6, and the elemental composition of the photocatalyst can be seen in Table 2.

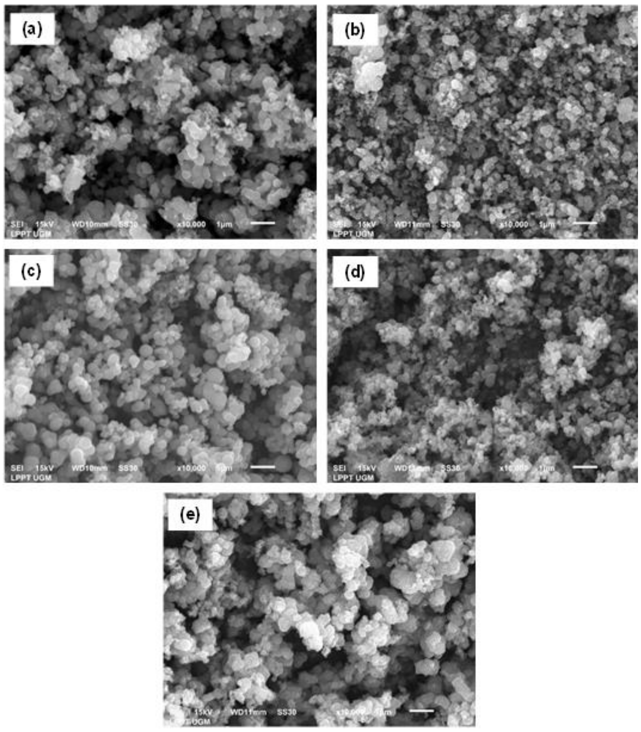

Figure 5. SEM images of (a) TiO_2, (b) $S_{2\%}$-TiO_2, (c) $S_{4\%}$-TiO_2, (d) $S_{10\%}$-TiO_2, and (e) $S_{20\%}$-TiO_2

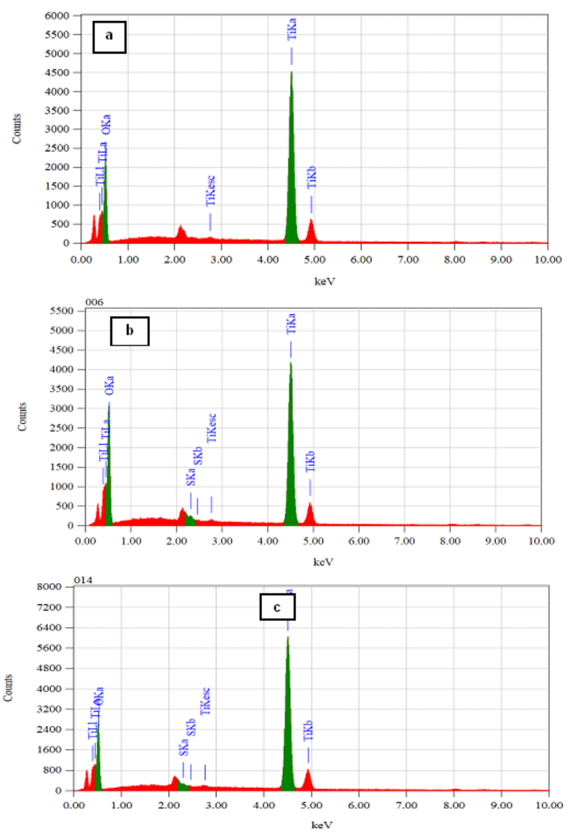

Figure 6. EDX spectrum of (a) TiO_2, (b) $S_{10\%}$-TiO_2, and (c) $S_{20\%}$-TiO_2

3.1.4. UV-vis SRS analysis

The optical properties and the band gap energy was identified by the UV-vis SRS spectrum. According to Figure 7(a), TiO_2 shows a very high absorption profile in UV light areas (200-400 nm) and negligible absorption in the visible light region (400-500 nm) since to the wide band gap of anatase titania (3.2 eV). Meanwhile, after S doping, the absorption showed a redshift to the visible region due to the formation of a new sub-bandgap above the VB resulting from doping S into TiO_2, thus, decrease the band gap energy, and the energy from visible light irradiation were able to excite the electrons from VB to CB. The extent of this shift was proportional to the increasing concentration of S dopant added to titania. To prove these results, the band gap energy before and after S doping of the photocatalyst was calculated by Tauc plot between $(\alpha h\upsilon)^2$ vs. $h\upsilon$. The TiO_2 band gap energy was identified to be 3.2 eV. After S doping, the band gap of $S_{2\%}$-TiO_2, $S_{4\%}$-TiO_2, $S_{10\%}$-TiO_2 and $S_{20\%}$-TiO_2 were found to be 3.28, 3.15, 3.16, and 3.20 respectively (Figure 7(b)). These results show that cationic S is able to reduce the band gap energy through the formation of new energy level from Ti−O−S bonds and is accordance with the previous reports (Devi and Kavitha, 2014; Chen *et al.*, 2017).

Table 2. The elements composition of TiO_2 and S-TiO_2 from EDX analysis

Element	% Atom				
	TiO_2	**$S_{2\%}$-TiO_2**	**$S_{4\%}$-TiO_2**	**$S_{10\%}$-TiO_2**	**$S_{20\%}$-TiO_2**
Ti	27.28	21.57	23.73	22.53	29.43
O	72.72	78.43	76.27	77.37	70.56
S		-	-	0.10	0.01

Table 3. Comparison of d-spacing obtained from SAED dan XRD analysis

Photocatalyst	2θ	hkl	*d*-spacing (Å)	
			XRD	**SAED**
TiO_2	25.21	101	3.53	3.59
	37.73	004	2.38	2.48
	47.95	200	1.89	1.97
	53.87	105	1.70	1.74
	54.97	211	1.67	1.56
	62.66	204	1.48	1.43
$S_{10\%}$−TiO_2	25.21	101	3.53	3.68
	37.90	004	2.37	2.51
	47.92	200	1.89	2.03
	53.87	105	1.70	1.80
	54.87	211	1.67	1.58
	62.78	204	1.47	1.42

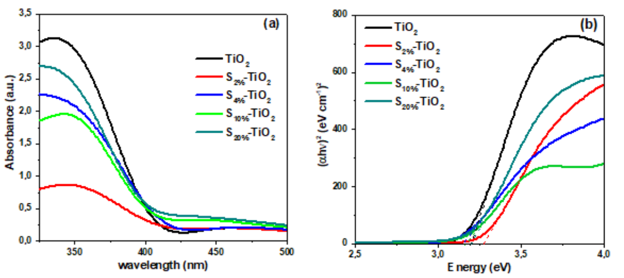

Figure 7. (a) UV-vis SRS spectrum and (b) Tauc's plot of TiO_2 and S-TiO_2

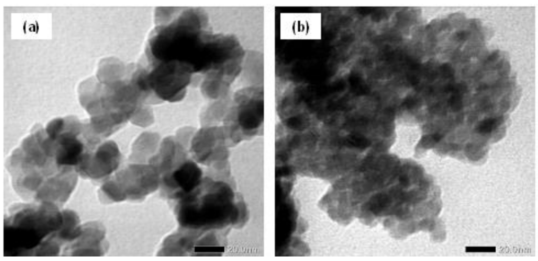

Figure 8. TEM images of (a) TiO_2 and (b) $S_{10\%}$-TiO_2

3.1.5. TEM analysis

According to the TEM images(Figure 8) both bare TiO_2 and $S_{10\%}$-TiO_2 displayed spherical-shaped formation and were homogeneously dispersed on the titania photocatalyst. These results are in accordance with the result of the SEM images.

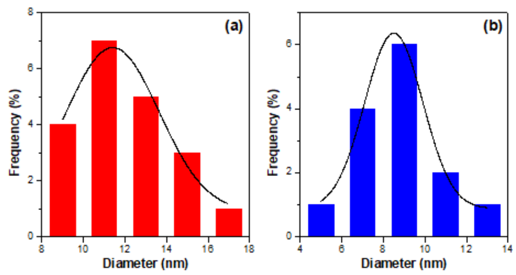

Figure 9. Particle distribution of (a) TiO_2 and (b) $S_{10\%}$−TiO_2

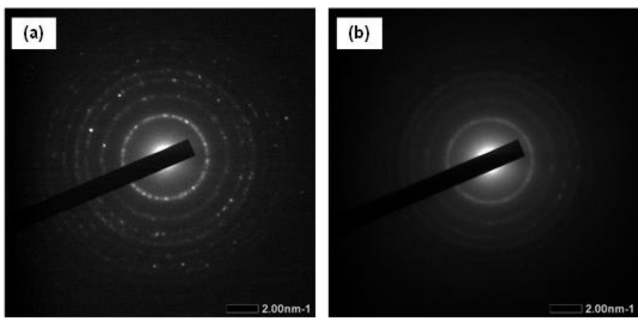

Figure 10. SAED patterns of (a) TiO_2 and (b) $S_{10\%}$−TiO_2 photocatalyst

The average particle size of bare TiO_2 were identified as 11.4 nm (Figure 9(a)). However, after the addition of a 10% concentration of S dopant, the average particle size decreased to 8.5 nm as showed in Figure 9(b). The decrease of particle size after the addition of S dopants indicates a small distortion in the crystal lattice of TiO_2 and also confirms the successful incorporation of S dopants into TiO_2.

Selected area diffraction (SAED) was used to ensure that the photocatalyst synthesized was anatase phase TiO_2. Based on Figure 10 (a) and (b), the SAED patterns of TiO_2 and $S_{10\%}$-TiO_2 showed the diffraction of the polycrystalline ring from reflection (101), (004), (200), (105), (211), and (204) anatase TiO_2, and the *d*-spacing generated from SAED corresponds to the *d*-spacing value obtained from XRD was summarizes in Table 3.

3.2. Photocatalytic degradation

3.2.1. Effect of different catalyst

The photocatalytic activity of photocatalyst before and after dopant addition was studied in the degradation of 20 mg L^{-1} RBB solution using two different types of light sources, visible and UV-light for 120 min of irradiation time. The results of photocatalytic degradation by various photocatalysts are shown in Figure 11.

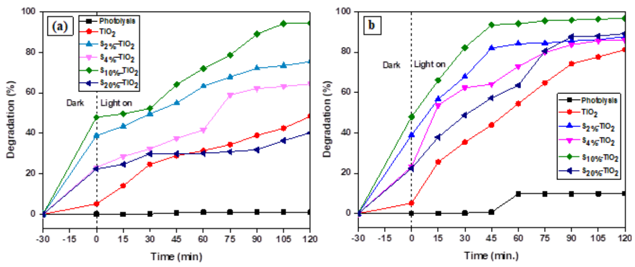

Figure 11. The effect of different photocatalysts on the degradation of RBB using (a) visible, and (b) UV-light irradiation, photocatalyst dosage: 1 g L^{-1}, pH: 5.5, and RBB concentration: 20 mg L^{-1}

As a comparison, the degradation of RBB without the addition of photocatalyst was also examined to find out the photolysis properties of RBB. The results showed that after 120 min of visible-light irradiation, RBB does not undergo degrade. However, a very small concentration decrease was observed after 60 min of UV exposure, then the concentration tends to constant even up to 120 min of irradiation, which demonstrated that the RBB is quite stable under sunlight. A very small degradation also observed when TiO_2 was added into the solution, even after 120 min of visible light irradiation, only 48% of the RBB can be degraded. Since the energy from visible light was not enough to initiate the excitation of the electrons from the VB to the CB of TiO_2, and •OH radicals were not optimally generated. Compared to TiO_2, the decoloration performance of S-TiO_2 was significantly increased both under visible and UV light. $S_{10\%}$-TiO_2 showed the best photocatalytic activity with the removal percentages of RBB was 94% and 96% after 120 min of visible and UV light exposure, respectively (Figure 11). Meanwhile, only 48% and 81% of RBB could be degraded by TiO_2 at the same light source and time. This result is in accordance with the band gap energy (Eg) from UV-Vis SRS, that $S_{10\%}$-TiO_2 has a smaller Eg than TiO_2 and corresponds to the energy of visible light irradiation.

$S_{2\%}$-TiO_2 (75% degradation) displayed the second good photocatalytic activity compared to $S_{4\%}$-TiO_2 (64% degradation) although the Eg of $S_{4\%}$-TiO_2 was slightly smaller than $S_{2\%}$-TiO_2. This may be due to the larger surface area of $S_{2\%}$-TiO_2 (Table 1), so the amount of pollutants adsorbed on the surface of $S_{2\%}$-TiO_2 is greater than $S_{4\%}$-TiO_2. Sulfur doping is known to cause a significant increase in the surface area of the photocatalyst. Moreover, the number of active sites will increase with increasing surface area. The large surface area of the catalyst can facilitate more hydroxyl groups of water molecules that are adsorbed where the hydroxyl groups can serve as trap holes to provide hydroxyl radicals (•OH) for pollutant degradation (Devi and Kavitha, 2014). Furthermore, RBB degradation by $S_{20\%}$-TiO_2 was not much different from TiO_2. Although Eg of $S_{20\%}$-TiO_2 (3.11 eV) is smaller than TiO_2 (3.2 eV), the particle size is much larger than TiO_2, suggesting that the addition of 20% dopant concentration causes agglomeration on the TiO_2 surface and inhibit light absorption for electron excitation process (Isari et al., 2018).

RBB degradation was initiated by the adsorption process followed by a photocatalytic reaction. To evaluate whether the adsorption process continues along with the photocatalytic process, catalyst adsorption of TiO_2 and $S_{10\%}$-TiO_2 was carried out in dark condition for 120 min without irradiation as shown in Figure 12. The adsorption process of these catalysts was continued until 15 min, then the RBB concentration tends to be constant, which implied that after 15 minutes of contact time, the process was photocatalytic degradation.

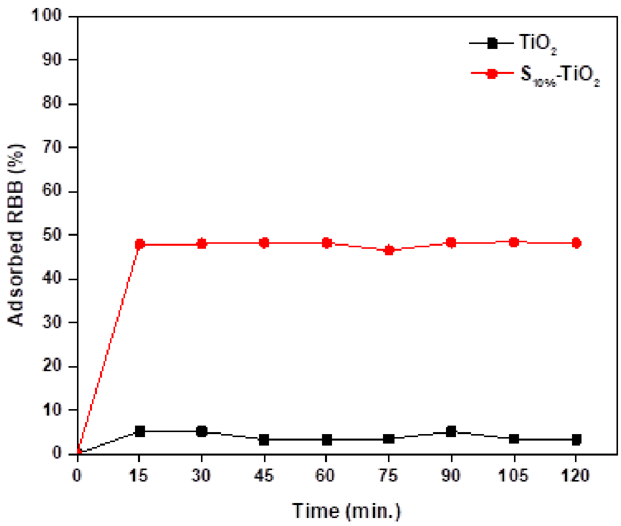

Figure 12. Adsorption of RBB by TiO_2 and $S_{10\%}$-TiO_2 in the dark condition at RBB concentration: 20 mg L^{-1}, initial pH 5.5, and photocatalyst dosage: 1 g L^{-1}

3.2.2. Effect of pH

The effect of pH is a pivotal parameter in the efficiency of the decolorization process because it can affect the photocatalyst surface, dye characteristics, and the rate of the degradation process. The effect of the initial pH on the

RBB degradation by $S_{10\%}$-TiO_2 catalyst under visible light exposure was evaluated in the range 2.0-10.0 as shown in Figure 13 (a).

According to Figure 13(a), the RBB degradation efficiency increased from 66.6% to 93% at 60 minutes when the initial pH was decreased from 4.0 to 3.0. However, the degradation efficiency decreased to 35.8%, 21.4%, and 18.1% while the pH increased to 8.0, 9.0, and 10.0, respectively. TiO_2 has different charges, positively or negatively, depend on the solution pH:

$$pH < pH_{ZPC}: Ti\text{-}OH + H^+ \rightarrow TiOH_2^+ \quad (3)$$

$$pH > pH_{ZPC}: Ti\text{-}OH + OH^- \rightarrow TiO^- + H_2O \quad (4)$$

From Figure 13(a), the optimum pH for RBB degradation is 3.0 while the pH of point zero charge (pH_{ZPC}) of TiO_2 is 6.8 (Muruganandham *et al.*, 2006). TiO_2 surface will be positively charged when the pH solution is below the pH_{ZPC}. Meanwhile, at acidic medium (pH = 3.0), RBB contains sulfonate (SO_3^-) and sulfite (SO_3^{2-}) groups which can be adsorbed properly through electrostatic force by the positively charged of TiO_2 surface as the beginning of the degradation process (Muruganandham *et al.*, 2006; Ghoreishian *et al.*, 2014). However, decreasing the solution pH to 2.0 did not show an increase in degradation efficiency compared to pH 3.0. Then, the degradation efficiency decreased as the pH increased from 7.0 to 10.0 due to in this condition, TiO_2 surface was negatively charged resulting in a repulsion with the dye charge.

3.2.3. Effect of $S_{10\%}$-TiO_2 dosage

Evaluation of photocatalytic performance with various catalyst doses was performed by varying the $S_{10\%}$-TiO_2 mass from 0.2 to 1.0 g L^{-1} (Figure 13(b)). Increased the photocatalyst dose from 0.2 to 0.8 g L^{-1} resulted in an increase in the degradation from 61% to 97%, since the surface area will increase with an increasing the number of catalyst, the dye adsorption rate and the hydroxyl radical formation on the surface will increase. However, the result did not rise significantly when the catalyst dose was increased to 1.0 g L^{-1}. It can be caused by the excessive amount of catalyst causing aggregation, thereby reducing the intensity of light entering the solution, which causes a decrease of the rate of radical formation for the degradation process.

3.2.4. Effect of dye concentration

The initial concentration of pollutants will affect the photocatalytic ability of $S_{10\%}$-TiO_2. For this purpose, the RBB concentration is varied from 20 to 50 mg L^{-1}. As shown in Figure 13(c), the degradation efficiency reduced from 97 to 67% when the dye concentration increased from 20 to 50 mg L^{-1}, which was associated with a higher of the dye concentration causing the number of negative charge molecules of RBB adsorbed on the catalyst surface is build-up, as consequence blocking the formation of reactive species due to deactivation of the active site of the catalyst. Also, at high concentration of dye, contaminant molecules adsorbed more photons which reduce the light intensity attacked by the catalyst (Isari *et al.*, 2018).

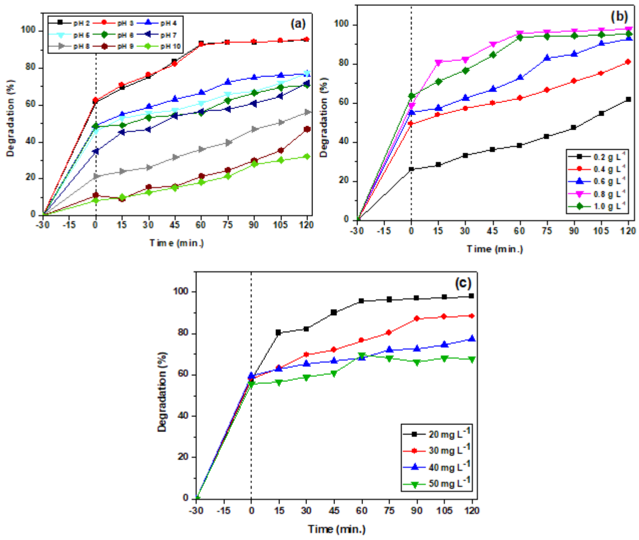

Figure 13. Influence of operational factors on photocatalytic degradation of RBB for 120 min visible light illumination by $S_{10\%}$-TiO_2 photocatalyst, (a) Effect of pH at photocatalyst dosage: 1 g L^{-1}, RBB concentration: 20 mg L^{-1}, (b) Effect of photocatalyst dosage at initial pH: 3.0, RBB concentration: 20 mg L^{-1}, and (c) Effect of RBB concentration at catalyst dosage: 0.8 g L^{-1}, pH: 3.0.

3.2.5. The recyclable ability of $S_{10\%}$-TiO_2 photocatalyst

Stability and reuse tests of $S_{10\%}$-TiO_2 photocatalyst material have been carried out. For each photocatalytic process, $S_{10\%}$-TiO_2 was centrifuged then washed and dried for reuse in the next process. Figure 14 shows the results of the photocatalyst recycling test with the same condition. The results showed a fairly high photodegradation efficiency and only slightly decreased by 19% after four cycles. Therefore, this study shows that this photocatalyst has good prospects and can be used repeatedly for decontaminate pollutants in water.

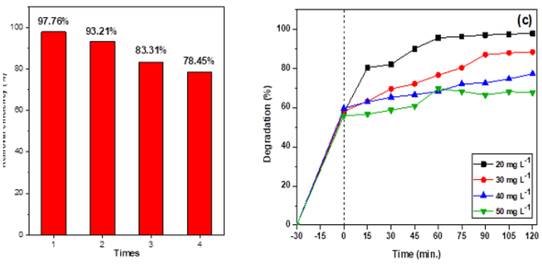

Figure 14. Recyclability of $S_{10\%}$-TiO_2 for RBB photocatalytic degradation under visible light illumination, RBB concentration: 20 mg L^{-1}, initial pH: 3.0, and photocatalyst dosage: 0.8 g L^{-1}

3.3. Kinetic study

Several kinetic model equations can be used to evaluate the kinetics of RBB photodegradation by $S_{10\%}$-TiO_2 and TiO_2 under solar illumination. The most suitable kinetics model will produce the greatest correlation coefficient (R^2). The reaction rate constant (k) of the photodegradation of RBB was studied using the Langmuir-Hinshelwood kinetic equation (Eq. 9), pseudo-first-order (PFO) (Eq. 10), and pseudo-second-order (PSO) (Eq. 11).

The Langmuir-Hinshelwood (L-H) kinetics model is the most widely used for evaluating the photocatalytic kinetics of chemical compounds on semiconductor surfaces using the L-H kinetics equation as follows (Sun *et al.*, 2018):

$$\frac{\ln\left(\frac{C_0}{C}\right)}{C_0 - C} = \frac{m}{V} k_{pm} K_{ads} \frac{t}{C_0 - C} - K_{ads} \quad (5)$$

where C_o is the initial dye concentration, C is the concentration at time t, m is the mass of the photocatalyst, V is the volume of the solution, Kpm is the photocatalytic reaction rate constant per unit mass of the photocatalyst, $Kads$ is the photocatalyst adsorption equilibrium constant, and t is the degradation time. The value for Kpm can be obtained from the slope and intercept of linear equation by the plot between $\ln(C_o/C)/(C_o-C)$ vs. $t/(C_o-C)$.

Table 4. Kinetics parameters of L-H, PFO, and PSO on RBB decontamination

Langmuir-Hinshelwood kinetics model			
Photocatalyst	k_{pm} **(mol g^{-1} min^{-1})**	K_{ads} **(m^3 mol^{-1})**	R^2
TiO_2	2.39×10^{-5}	51.30	0.870
$S_{10\%}$-TiO_2	3.0×10^{-4}	47.78	0.694
Pseudo first order kinetic model			
	k_1 (min^{-1})	q_e **(mg g^{-1})**	R^2
TiO_2	0.017	9.55	0.986
$S_{10\%}$-TiO_2	0.028	17.98	0.934
Pseudo second order kinetics model			
	k_2 **(g mg^{-1} min^{-1})**	q_e **(mg g^{-1})**	R^2
TiO_2	0.8869	13.10	0.870
$S_{10\%}$-TiO_2	0.9461	17.78	0.938

The experimental data was also applied to the PFO kinetics equation (Eq. 6):

$$\ln\frac{q_e}{q_e - q_t} = k_1 t \quad (6)$$

where q_e is the amount of substrate adsorbed per unit mass of catalyst at equilibrium (mg g^{-1}), q_t is the amount of substrate adsorbed per unit mass of catalyst at time t (mg g^{-1}). From Eq. 10, a linear curve can be made between $\ln\frac{q_e}{q_e - q_t}$ vs. t, the slope value is obtained which is the constant rate of photodegradation RBB (k_1) (Figure 15(b) (Tan and Hameed, 2017).

Then, PSO kinetics equation is also used:

$$\frac{t}{q_t} = \frac{1}{k_2 q_e^2} + \frac{1}{q_e} t \quad (7)$$

where k_2 is the PSO rate constant (g mg^{-1} min^{-1}). The value of k_2 can be obtained from plot linear between t/q_t vs. t (Figure 15(c)).

The correlation coefficient (R^2) value obtained from the PSO is greater than the L-H and PFO kinetics model, which indicates that the photodegradation of RBB by $S_{10\%}$-TiO_2 follows PSO kinetics model, where the degradation rate is influenced by the concentration of RBB and the active group on the photocatalyst surface. The values of L-H, PFO, and PSO parameters of the evaluation results are summarized in Table 4.

3.4. Mechanism of RBB photodegradation

Photocatalytic reactions can occur when TiO_2 absorbs photons from illumination that have a wavelength greater than the band gap energy. The characterization result show that S-doped TiO_2 has been successfully synthesized. S doping caused the bandgap narrowing of TiO_2 thereby increasing visible light activity of the photocatalyst. A schematic of the photocatalytic mechanism by $S_{10\%}$-TiO_2 is shown in Figure 16. When $S_{10\%}$-TiO_2 is exposed to visible light, the electrons in the VB will be moved towards the CB (e_{CB}^-) and produce holes (h_{VB}^+) in the VB. These excited electrons and hole pairs are commonly known as excitons (Islam *et al.*, 2020).

$$S\text{-}TiO_2 + hv \rightarrow h_{VB}^+ + e_{CB}^- \quad (8)$$

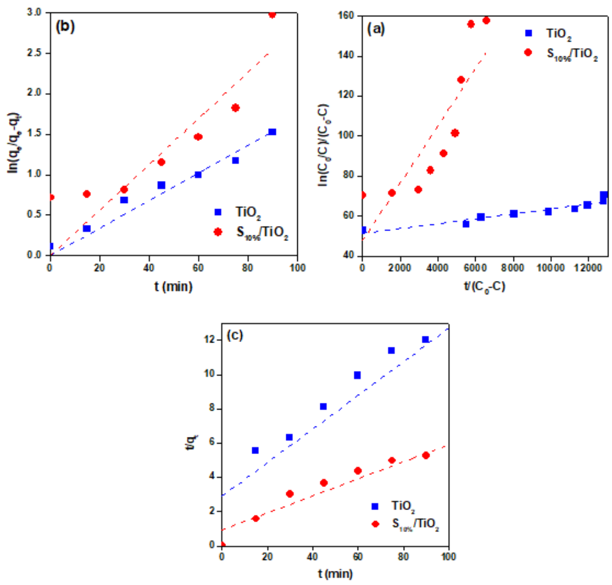

Figure 15. Plots of (a) L-H (b) PFO, and (c) PSO models for photocatalytic degradation of RBB by TiO_2 and $S_{10\%}$-TiO_2, RBB concentration: 20 mg L^{-1}, initial pH: 5.5, and photocatalyst dosage: 1.0 g L^{-1}

The holes can be reacted with adsorbed hydroxyl anion in the TiO_2 surface to produce hydroxyl radicals which have strong oxidizing power to decompose organic pollutants, and excited electrons (e_{CB}^-) can reduce O_2 to form oxygen radicals which can be converted into hydroxyl radicals in water.

$$OH^- + h_{VB}^+ \rightarrow \bullet OH \quad (9)$$

$$\bullet OH + RBB \rightarrow \text{degradation pollutant } (Cl^-, NO_3^-, SO_4^{2-}, CO_2 \text{ and } H_2O) \quad (10)$$

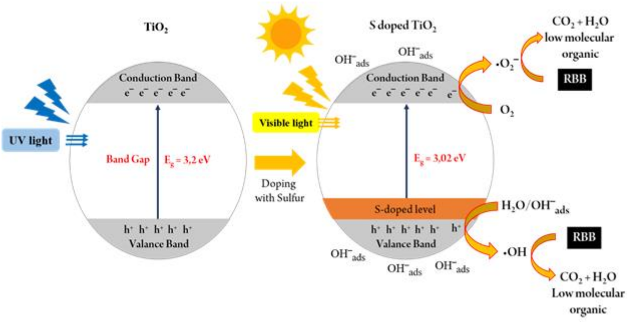

Figure 16. Schematic mechanism of S-doped TiO_2 for photocatalytic degradation of RBB

4. Conclusion

The decolorization of Remazol Black (RBB) was investigated using a S-TiO_2 photocatalyst. Characterization using XRD, FT-IR, SEM-EDX, UV-Vis SRS, and TEM showed that S-doped TiO_2 has been successfully synthesized and was able to degrade RBB under visible light illumination better than bare TiO_2. 10% (w/w) S was the optimum concentration that increased the photocatalytic activity of TiO_2 to the visible region, which resulted in the largest reduction in the bandgap to 3.02 eV. 94% decolorization was achieved by $S_{10\%}$-TiO_2 while bare TiO_2 was only able to degrade 48% RBB for 120 minutes of visible light exposure. Parameters affecting the effectiveness of catalytic decolorization have been studied. The best results were obtained at pH solution of 3.0, and photocatalyst dose of 0.8 gL^{-1}. In general, by increasing RBB concentration, the rate of photocatalytic degradation decreases, and kinetic analysis shows that the decolorization followed the pseudo-second-order kinetic model.

Acknowledgements

This research was financially supported by Kemenristekdikti (Ministry of Research, Technology and Higher Education) of Indonesia through the Pendidikan Magister menuju Doktor untuk Sarjana Unggul (PMDSU) Scholarship Program (No. 3140/UN1/DITLIT/DIT-LIT/LT/2020).

References

Abu S. and Ribeiro C. (2016), An insight toward the photocatalytic activity of S doped 1-D TiO_2 nanorods prepared via novel route: As promising platform for environmental leap, *Journal of Molecular Catalysis A: Chemical*, **412**, 78–92.

Ahmad M.A. and Rahman N.K. (2011), Equilibrium, kinetics and thermodynamic of Remazol Brilliant Orange 3R dye adsorption on coffee husk-based activated carbon, *Chemical Engineering Journal*, **170**, 154–161.

Aksu Z. and Akın A.B. (2010), Comparison of Remazol Black B biosorptive properties of live and treated activated sludge, *Chemical Engineering Journal*, **165**, 184–193.

Akti F. (2018), Photocatalytic degradation of remazol yellow using polyaniline–doped tin oxide hybrid photocatalysts with diatomite support, *Applied Surface Science*, **455**, 931–939.

Alvarez P.J.J., Chan C.K., Elimelech M., Halas N.J. and Villagrán D. (2018), Emerging opportunities for nanotechnology to enhance water security, *Nature Nanotechnology*, **13**, 634–641.

Asiri A.M., Al-amoudi M.S., Bazaid S.A., Adam A.A., Alamry K.A. and Anandan S. (2014), Enhanced visible light photodegradation of water pollutants over N- , S-doped titanium dioxide and n-titanium dioxide in the presence of inorganic anions, *Journal of Saudi Chemical Society*, **18**, 155–163.

Bessergenev V.G., Mateus M. C., Botelho A.M., Hantusch M. and Burkel E. (2015), An improvement of photocatalytic activity of TiO_2 Degussa P25 powder, *Applied Catalysis A: General*, **500**, 40–50.

Chaudhuri R.G. and Paria S. (2014), Visible light induced photocatalytic activity of sulfur doped hollow TiO_2 nanoparticles, synthesized via a novel route, *Dalton Transactions*, **43**, 5526–5534.

Chen C., Cheng M. and Chen A. (2012), Photocatalytic decolorization of Remazol Black 5 and Remazol Brilliant Orange 3R by mesoporous TiO_2, *Journal of Environmental Management*, **102**, 125–133.

Chen X., Kuo D. and Lu D. (2017), Visible light response and superior dispersed S-doped TiO_2 nanoparticles synthesized via ionic liquid, *Advanced Powder Technology*, **28**, 1213–1220.

Chen X., Sun H., Zhang J., Guo Y. and Kuo D. (2019), Cationic S-doped TiO_2/SiO_2 visible-light photocatalyst synthesized by co-hydrolysis method and its application for organic degradation, *Journal of Molecular Liquids*, **273**, 50–57.

Chen Z., Ma J., Yang K., Feng S., Tan W. and Tao Y. (2017), Preparation of S-doped TiO_2-three dimensional graphene aerogels as a highly efficient photocatalyst, *Synthetic Metals*, **231**, 51–57.

Devi L.G. and Kavitha R. (2014), Enhanced photocatalytic activity of sulfur doped TiO_2 for the decomposition of phenol: A new insight into the bulk and surface modification, *Materials Chemistry and Physics*, **143**, 1300–1308.

Eskandari P., Farhadian M., Nazar A.R.S. and Jeon B. (2019), Adsorption and photodegradation efficiency of TiO_2/Fe_2O_3/PAC and TiO_2/Fe_2O_3/Zeolite nanophotocatalyst for the removal of cyanide, *Industrial & Engineering Chemistry Research*, **58**, 2099–2112.

Ghoreishian S.M., Badii K., Norouzi M., Rashidi A., Montazer M., Sadeghi M. and Vafaee M. (2014), Decolorization and mineralization of an azo reactive dye using loaded nano-photocatalysts on spacer fabric: Kinetic study and operational factors, *Journal of the Taiwan Institute of Chemical Engineers*, **4**, 2436–2446.

Hamadanian M. and Majedi A. (2009), Preparation and characterization of S-doped TiO_2 nanoparticles , effect of calcination temperature and evaluation of photocatalytic activity, *Materials Chemistry and Physics*, **116**, 376–382.

Han C., Andersen J., Likodimos V., Falaras P., Linkugel J. and Dionysiou D.D. (2014), The effect of solvent in the sol–gel synthesis of visible light-activated, sulfur-doped TiO_2 nanostructured porous films for water treatment, *Catalysis Today*, **224**, 132–139.

Han C., Pelaez M., Likodimos V., Kontos A.G., Falaras P., O'Shea K. and Dionysiou D.D. (2011), Innovative visible light-activated sulfur doped TiO_2 films for water treatment, *Applied Catalysis B: Environmental*, **107**, 77–87.

Isari A.A., Payan A., Fattahi M., Jorfi S. and Kakavandi B. (2018), Photocatalytic degradation of rhodamine B and real textile wastewater using Fe-doped TiO_2 anchored on reduced graphene oxide (Fe-TiO_2/rGO): Characterization and feasibility, mechanism and pathway studies, *Applied Surface Science*, **462**, 549–564.

Islam M.T., Dominguez A., Turley R.S., Kim H., Sultana K.A., Shuvo M., Alvarado-tenorio B., Montes M.O., Lin Y., Gardea-torresdey J. and Noveron J.C. (2020), Development of photocatalytic paint based on TiO_2 and photopolymer resin for the degradation of organic pollutants in water, *cience of The Total Environment*, **704**, 135406.

Kumar K.M., Godavarthi S., Karthik T.V.K., Mahendhiran M., Hernandez-eligio A., Hernandez-como N., Agarwal V. and Gomez L.M. (2016), Green synthesis of S-doped rod shaped anatase TiO_2 microstructures, *Materials Letters*, **183**, 211–214.

Lin Y.H., Hsueh H.T., Chang C.W. and Chu H. (2016), The visible light-driven photodegradation of dimethyl sulfide on S-doped TiO_2: Characterization, kinetics, and reaction pathways, *Applied Catalysis B: Environmental*, **199**, 1–10.

Marques S.M., Tavares C.J., Oliveira L.F. and Oliveira-campos A.M.F. (2010), Photocatalytic degradation of C.I. Reactive Blue 19 with nitrogen-doped TiO_2 catalysts thin films under UV/visible light, *Journal of Molecular Structure*, **983**, 147–152.

Mcmanamon C., O'Connell J., Delaney P., Rasappa S., Holmes J.D. and Morris M.A. (2015), A facile route to synthesis of S-doped TiO_2 nanoparticles for photocatalytic activity, *Journal of Molecular Catalysis A: Chemical*, **406**, 51–57.

Murcia J.J., Hidalgo M.C., Navío J.A., Arana J. and Dona-Rodríguez J.M. (2015), Study of the phenol photocatalytic degradation over TiO_2 modified by sulfation, fluorination, and platinum nanoparticles photodeposition, *Applied Catalysis B: Environmental*, 179, 305–312.

Muruganandham M. and Swaminathan M. (2006), Advanced oxidative decolourisation of Reactive Yellow processes—a comparative study, *Separation and Purification Technology*, **48**, 297–303.

Muruganandham M., Sobana N. and Swaminathan M. (2006), Solar assisted photocatalytic and photochemical degradation of Reactive Black 5, *Journal of Hazardous Materials*, 137, 1371–1376.

Olowoyo J.O., Kumar M., Jain S.L., Shen S., Zhou Z., Mao S.S., Vorontsov A.V. and Kumar U. (2018), Reinforced photocatalytic reduction of CO_2 to fuel by efficient S-TiO_2 : Significance of sulfur doping, *International Journal of Hydrogen Energy*, 1–14.

Pereira L.D.O., Moura S.G.De, Coelho G.C.M., Oliveira L.C.A., Almeida E.T.De and Magalhães F. (2019), Magnetic photocatalysts from industrial residues and TiO_2 for the degradation of organic contaminants, *Journal of Environmental Chemical Engineering*, **7**, 102826.

Rauf M.A., Meetani M.A. and Hisaindee S. (2011), An overview on the photocatalytic degradation of azo dyes in the presence of TiO_2 doped with selective transition metals, *Desalination*, **276**, 13–27.

Sahel K., Bouhent M., Belkhadem F., Ferchichi M., Dappozze F., Guillard C. and Figueras F. (2014), Photocatalytic degradation of anionic and cationic dyes over TiO_2 P25, and Ti-pillared clays and Ag-doped Ti-pillared clays, *Applied Clay Science*, **95**, 205–210.

Sahel K., Perol N., Dappozze F., Bouhent M., Derriche Z. and Guillard C. (2010), Photocatalytic degradation of a mixture of two anionic dyes: Procion Red MX-5B and Remazol Black 5 (RB5), *Journal of Photochemistry and Photobiology A: Chemistry*, **212**, 107–112.

Siddiqa A., Masih D., Anjum D. and Siddiq M. (2015), Cobalt and sulfur co-doped nano-size TiO_2 for photodegradation of various dyes and phenol, *Journal of Environmental Sciences*, **37**, 100–109.

Sun P., Zhang J., Liu W., Wang Q. and Cao W. (2018), Modification to L-H Kinetics Model and Its Application in the Investigation on Photodegradation, *Catalysts*, **8**, 326–340.

Szatmáry L., Bakardjieva S., Subrt J., Bezdiˇ P., Brezová V. and Korenko M. (2011), Sulphur doped nanoparticles of TiO_2, *Catalysis Today*, **161**, 23–28.

Tan K.L. and Hameed B.H. (2017), Insight into the adsorption kinetics models for the removal of contaminants from aqueous solutions, *Journal of the Taiwan Institute of Chemical Engineers*, **74**, 25–48.

Tian G., Pan K., Fu H., Jing L. and Zhou W. (2009), Enhanced photocatalytic activity of S-doped TiO_2–ZrO_2 nanoparticles under visible-light irradiation, *Journal of Hazardous Materials*, **166**, 939–944.

Wahyuni E.T., Yulikayani P.Y. and Aprilita N.H. (2020), Enhancement of visible-light photocatalytic activity of Cu-doped TiO_2 for photodegradation of amoxicillin in water, *Journal of Materials and Environmental Science*, **11**, 670–683.

Wu M., Wu P., Lin T. and Lin T. (2018), Photocatalytic performance of Cu-doped TiO_2 nanofibers treated by the hydrothermal synthesis and air-thermal treatment, *Applied Surface Science*, **430**, 390–398.

Yi C., Liao Q., Deng W., Huang Y., Mao J., Zhang B. and Wu G. (2019), The preparation of amorphous TiO_2 doped with cationic S and its application to the degradation of DCFs under visible light irradiation, *Science of the Total Environment*, **684**, 527–536.

Yilmaz P., Lacerda A.M., Larrosa I. and Dunn S. (2017), Photoelectrocatalysis of Rhodamine B and Solar Hydrogen Production by TiO_2 and Pd/TiO_2 Catalyst Systems, *Electrochimica Acta*, **231**, 641–649.

Zhu M., Zhai C., Qiu L., Lu C., Paton A.S., Du Y. and Goh M.C. (2015), New method to synthesize S-doped TiO_2 with stable and highly efficient photocatalytic performance under indoor sunlight irradiation, *ACS Sustainable Chemistry & Engineering*, **3**, 3123–3129.